Reduced-order Models of Series Resonant Inverters in Induction Heating Applications

Alberto Dominguez, *Student Member, IEEE*, Luis Angel Barragan, Jose Ignacio Artigas,
Aranzazu Otin, *Member, IEEE*, Isidro Urriza, Denis Navarro.

Abstract-- **From the controller design framework, a simple analytical model that captures the dominant behavior in the range of interest is the optimal. When modeling resonant circuits, complex mathematical models are obtained. These high-order models are not the most suitable for controller design. Although some assumptions can be made for simplifying these models, variable frequency operation or load uncertainty can make these premises no longer valid. In this work, a systematic modeling order reduction technique, Slowly Varying Amplitude and Phase (SVAP), is considered for obtaining simpler analytical models of resonant inverters. SVAP gives identical results as the classical model-order residualization technique from automatic control theory. A slight modification of SVAP, Slowly Varying Amplitude Derivative and Phase (SVADP) is applied in this paper to obtain a better validity range. SVADP is validated for a half-bridge series resonant inverter (HBSRI) and for a high-order plant, a dual-half bridge series resonant inverter (DHBSRI) giving analytical second-order transfer functions for both topologies. Simulation and experimental results are provided to show the validity range of the reduced-order models.**

Index Terms-- **Reduced order Systems, Resonant inverters, Home Appliances, Induction Heating.**

I. INTRODUCTION

RESONANT inverters are more and more used in biomedical, lighting, and induction heating applications due to its superior efficiency and higher power density compare to non-resonant topologies. Despite their clear advantages, their behavior is a little more complex because of their greater harmonic content and load dependency.

Classical modeling techniques for pulse width modulation (PWM) converters are no longer valid for resonant topologies because of their close ratio between switching frequency and the resonant-tank natural frequency. Due to this dominant oscillatory nature, a generalized state-space averaging (GSSA) modeling technique was proposed in [1] as a natural extension of SSA for resonant topologies under the assumptions of first harmonic and slowly varying frequency. A similar modeling technique based on phasor transformation, more natural in AC circuit analysis, was proposed in [2, 3]. Lately, this technique has been called dynamic phasor modeling, and it has been

applied successfully to PWM systems [4] including an arbitrary number of harmonics. Essentially, all these techniques consider a Fourier series expansion of the system over a moving time window where the *k*-sliding harmonics or *k*-phasors are the new state variables. In order to take into account frequency-modulated resonant topologies, a modified phasor transformation was proposed in [5]. This phase-based phasor transformation considers both envelope and frequency variations and it has been successfully applied to LCC ballast inverters [5, 6] or recently in multi-generators in electrical power systems [7]. Direct dynamical enveloping [8, 9] is a more circuit oriented approach for modeling envelope signals in resonant inverters that provides identical results to those of phase-based phasor transformation. Extended Describing Function (EDF) was proposed in [10]. It was the first generalized multivariable modeling technique to include in a systematic way a limited number of harmonics including the possibility of modeling frequency-modulated topologies. The equivalent circuit model derived from EDF for a series resonant converter (SRC) is recognized to be the most successful one [11]. These techniques provide accurate models up to half the switching frequency. Sample-data modeling techniques are even more accurate and their validity range extends up to the switching frequency [12, 13]. However, these discrete-time small signal models are mostly provided numerically due to their mathematical complexity.

Although dynamic phasor and EDF techniques provide quite accurate results, it is known that they result in high-order models because of the sine and cosine parts separation of each state variable increasing the state matrix size. This order augmentation produces high-frequency poles and zeroes beyond the Nyquist frequency which are not representative of the sought model. Although these high-frequency terms can be dropped out, analytical transfer functions are difficult to be obtained even for a simple series resonant inverter (SRI). For induction heating applications, in [14, 15] the small-signal model of a phase-shift and frequency controlled SRI by EDF are presented respectively, in [16] the small-signal model of a dual half bridge series resonant inverter (DHBSRI) by EDF is provided, in [17-19] a small-signal model of a half-bridge series resonant inverter (HBSRI) by phase-based phasor transformation is obtained. However, neither [14-16] nor [17-19] provides analytical transfer functions.

For optimal controller design and robust performance it would be quite desirable to dispose of simpler analytical models. Some intuitive approximations consist in neglecting the influence of certain non-dominant elements [6, 20]. For mixed systems with slow and fast variables, an assumption

extensively applied is based on separating the system dynamics of different nature by singular perturbation theory [21]. This approach has been extensively applied in converters having both DC and AC stages [22] or converters operating in Discontinuous Conduction Mode (DCM) [23]. A similar approach is the equivalent current injected method that replaces the considered static variable as a function of the other system variables [24]. However, a more systematic approach would be more appropriate if previous assumptions do not hold. Model-order reduction techniques appear as a useful tool when the order of the plant to be controlled is too complex with regards to practical controller implementation [25]. These techniques consist in capturing the dominant behavior and neglecting those energy states which contribute less [25, 26]. However they usually require numerical computations that do not easily provide analytical expressions.

This work is focused on induction heating applications, where variable frequency operation and load uncertainty are the main obstacles for obtaining simple analytical models. This work is an extension of [27] where a reduced-order model of a HBSRI is obtained by residualization. This technique is a classical reduced-order modeling technique in automatic control systems [25]. In this paper, it's shown that residualization of series resonant capacitor voltage is identical to Slowly Varying Amplitude and Phase (SVAP) approach [22]. In order to provide better dynamic results than residualization in [27], a Slowly Varying Amplitude Derivative and Phase (SVADP) technique is proposed. The obtained results match with the ones recently published in [11] for a SRC. The aim of this paper is to apply SVADP as a systematic model-order reduction technique to resonant inverters to obtain simpler analytical models. The paper is organized as follows: Section II explains the SVAP and SVADP techniques in order to obtain the HBSRI reduced-order model. Section III reports the reduced-order model of a DHBSRI showing the easy extension of SVADP to high-order plants. For both resonant topologies, second order analytical transfer functions considering different control inputs and outputs are given for the first time in the literature. Simulation and experimental results are reported in Section IV showing the reduced-order models validity range. Finally, Section V reports some conclusions.

II. HBSRI MODEL REDUCTION WITH SVADP METHOD

Let consider a HBSRI driven by a square excitation voltage (e.g., the output voltage of a half-bridge inverter, Fig. 1). The excitation voltage is characterized by a constant dc input voltage V_g, angular switching frequency ω_S, and duty cycle d. The state equation in terms of the inductor current i_L, the capacitor voltage v_C, and the excitation voltage u is:

$$\frac{d}{dt}\begin{pmatrix} i_L \\ v_C \end{pmatrix} = \begin{pmatrix} -R/L & -1/L \\ 1/C & 0 \end{pmatrix}\begin{pmatrix} i_L \\ v_C \end{pmatrix} + \begin{pmatrix} 1/L \\ 0 \end{pmatrix} u \tag{1}$$

Assuming 1st harmonic approximation, the state variables and the excitation voltage can be written as:
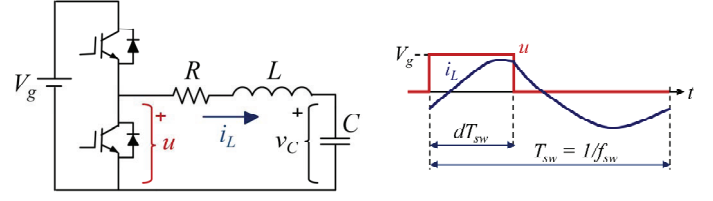
Fig. 1. HBSRI (a) schematic, (b) main waveforms.

$$i_L(t) = i_{Lc}(t)\cos(\omega_s t) + i_{Ls}(t)\sin(\omega_s t) \tag{2}$$

$$v_C(t) = v_{C0} + v_{Cc}(t)\cos(\omega_s t) + v_{Cs}(t)\sin(\omega_s t) \tag{3}$$

$$u(t) = u_0 + u_c(t)\cos(\omega_s t) + u_s(t)\sin(\omega_s t) \tag{4}$$

where u_c and u_s are obtained from the Fourier series decomposition of the square excitation voltage as:

$$\begin{pmatrix} u_c \\ u_s \end{pmatrix} = \frac{V_g}{\pi}\begin{pmatrix} \sin(2\pi d) \\ 1-\cos(2\pi d) \end{pmatrix} \tag{5}$$

Substituting (2)-(4) in (1) and applying harmonic balance, the following equation system is obtained:

$$\frac{d\mathbf{x}}{dt} = \mathbf{A}\cdot\mathbf{x} + \mathbf{B}\cdot V_g \tag{6}$$

where

$$\mathbf{x} = \begin{pmatrix} i_{Lc} & i_{Ls} & v_{Cc} & v_{Cs} \end{pmatrix}^T \tag{7}$$

$$\mathbf{A} = \begin{pmatrix} -R/L & -\omega_s & -1/L & 0 \\ \omega_s & -R/L & 0 & -1/L \\ 1/C & 0 & 0 & -\omega_s \\ 0 & 1/C & \omega_s & 0 \end{pmatrix} \tag{8}$$

$$\mathbf{B} = \frac{V_g}{\pi L}\begin{pmatrix} \sin(2\pi d) & 1-\cos(2\pi d) & 0 & 0 \end{pmatrix}^T \tag{9}$$

Although the assumption of 1st harmonic content is only strictly valid when the resonant tank is high-Q selective and when ω_S is quite near resonance, the dynamics of the resonant inverter are well predicted with only the 1st harmonic [15, 28]. The steady-state or equilibrium operating point $\mathbf{x}_e$ is obtained by imposing $d\mathbf{x}/dt = 0$ in (6):

$$\mathbf{x}_e = -\mathbf{A}^{-1}\mathbf{B}V_g = \begin{pmatrix} I_{Lc} & I_{Ls} & V_{Cc} & V_{Cs} \end{pmatrix}^T \tag{10}$$

$$I_{Lc} = \frac{V_g}{\pi}\frac{R\sin(2\pi D) - X(1-\cos(2\pi D))}{Z^2},$$
$$I_{Ls} = \frac{V_g}{\pi}\frac{X\sin(2\pi D) + R(1-\cos(2\pi D))}{Z^2} \tag{11}$$

$$V_{Cc} = -\frac{I_{Ls}}{C\Omega_S}, \quad V_{Cs} = \frac{I_{Lc}}{C\Omega_S} \qquad (12)$$

where X and Z are the reactance and impedance respectively of the series RLC at the steady-state angular switching frequency Ω_s and D is the steady-state duty cycle.

$$X = L\Omega_s - 1/(C\Omega_s) \qquad (13)$$

$$Z = \sqrt{R^2 + X^2} \qquad (14)$$

Assuming small signal perturbation and neglecting higher order terms, the EDF small-signal model near $\mathbf{x}_e$ can be expressed as:

$$\frac{d}{dt}\widehat{\mathbf{x}} = \mathbf{A}\widehat{\mathbf{x}} + \mathbf{B}_\omega\widehat{\omega}_s + \mathbf{B}_d\widehat{d} \qquad (15)$$

where:

$$\widehat{\mathbf{x}} = \begin{bmatrix} \widehat{i}_{Lc} & \widehat{i}_{Ls} & \widehat{v}_{Cc} & \widehat{v}_{Cs} \end{bmatrix}^T \qquad (16)$$

$$\mathbf{B}_\omega = \frac{d\mathbf{A}}{d\omega_s}\mathbf{x}\bigg|_{\mathbf{x}_e} = \begin{bmatrix} -I_{Ls} & I_{Lc} & -V_{Cs} & V_{Cc} \end{bmatrix}^T \qquad (17)$$

$$\mathbf{B}_d = \frac{\partial\mathbf{B}}{\partial d}V_g\bigg|_{\mathbf{x}_e} = \frac{2V_g}{L}\begin{bmatrix} \cos(2\pi D) & \sin(2\pi D) & 0 & 0 \end{bmatrix}^T \qquad (18)$$

The variables with a hat represent small deviations with respect the equilibrium, uppercase variables represent steady-state ones.

A. Model-order reduction with SVAP and SVADP approaches

The system order is defined by the size of the state matrix $\mathbf{A}$. In order to reduce it, some state equations have to be removed. Let's consider a simple system expressed in the state-variable form as follows:

$$\begin{pmatrix} d\mathbf{x}_1/dt \\ d\mathbf{x}_2/dt \end{pmatrix} = \begin{pmatrix} \mathbf{A}_{11} & \mathbf{A}_{12} \\ \mathbf{A}_{21} & \mathbf{A}_{22} \end{pmatrix} \cdot \begin{pmatrix} \mathbf{x}_1 \\ \mathbf{x}_2 \end{pmatrix} + \begin{pmatrix} \mathbf{B}_1 \\ \mathbf{B}_2 \end{pmatrix}\mathbf{u} \qquad (19)$$

Let's assume that we are able to obtain a linear function that relates the dynamic terms of both state variables sets $\mathbf{x}_1$, $\mathbf{x}_2$ as follows:

$$\frac{d\mathbf{x}_2}{dt} = \mathbf{F}\frac{d\mathbf{x}_1}{dt} \qquad (20)$$

We can substitute (20) in the second equation of (19) to obtain the following linear function:

$$\mathbf{x}_2 = \mathbf{A}_{22}^{-1}(\mathbf{F}\frac{d\mathbf{x}_1}{dt} - \mathbf{A}_{21}\mathbf{x}_1 - \mathbf{B}_2\mathbf{u}) \qquad (21)$$

From (21) and (19) we can obtain the following reduced-order model of the state variables set $\mathbf{x}_1$ of interest:

$$\frac{d\mathbf{x}_1}{dt} = (\mathbf{I} - \mathbf{A}_{12}\mathbf{A}_{22}\mathbf{F})^{-1}((\mathbf{A}_{11} - \mathbf{A}_{12}\mathbf{A}_{22}^{-1}\mathbf{A}_{21})\mathbf{x}_1 +$$
$$(\mathbf{B}_1 - \mathbf{A}_{12}\mathbf{A}_{22}^{-1}\mathbf{B}_2)\mathbf{u}) \qquad (22)$$

This reduced-order model preserves the steady-state gain of the system. The key idea is to know how to obtain (20) in a simple and systematic way. Since we are interested in obtaining low-frequency models, we can consider slowly varying functions of time as suitable approximations to obtain functions like (20) to finally reduce the order of the system. SVAP approach has been traditionally used to study oscillatory systems. This approach relies on assuming slowly varying amplitude and phase of a state variable [1, 22]. Since we are interested in current and power transfer functions, the state variables of interest will be $x_1 = (i_{Lc}, i_{Ls})$ and the state variables to be substituted $x_2 = (v_{Cc}, v_{Cs})$. Let's consider the series capacitor voltage and its time derivative expressions as:

$$v_C(t) = v_{C0} + v_{C1}(t)\sin(\omega_s t + \phi(t)) \qquad (23)$$

$$\frac{dv_C}{dt} = \frac{dv_{C1}}{dt}\sin(\omega_s t + \phi(t)) + v_{C1}(\omega_s + \frac{d\phi(t)}{dt})\cos(\omega_s t + \phi(t)) \qquad (24)$$

The SVAP approach relies on assuming amplitude v_{C1} and phase $\phi(t)$ as slowly varying functions of time ($dv_{C1}/dt = 0$, $d\phi/dt = 0$). Under these assumptions (24) and i_L can be expressed as:

$$\frac{dv_C}{dt} = v_{C1}\omega_s\cos(\omega_s t + \phi(t)) \qquad (25)$$

$$i_L = C\frac{dv_C}{dt} = v_{C1}C\omega_s\cos(\omega_s t + \phi(t)) \qquad (26)$$

Since we prefer to work with sine and cosine parts of state variables as (3) instead of amplitude and phase because it is more natural to EDF modeling approach, (23, 24) can be rearranged as:

$$v_C(t) = v_{C0} + v_{Cc}\cos(\omega_s t) + v_{Cs}\sin(\omega_s t) \qquad (27)$$

$$\frac{dv_C}{dt} = (\frac{dv_{Cc}}{dt} + v_{Cs}\omega_s)\cos(\omega_s t) + (\frac{dv_{Cs}}{dt} - v_{Cc}\omega_s)\sin(\omega_s t) \qquad (28)$$

where:

$$v_{Cc} = v_{C1}\sin(\phi(t)), \quad v_{Cs} = v_{C1}\cos(\phi(t)) \qquad (29)$$

The model order residualization technique of the series resonant capacitor voltage [25, 27] assumes that both v_{Cc} and v_{Cs} are slowly varying functions of time

($dv_{Cc}/dt = 0$, $dv_{Cs}/dt = 0$). Under these premises (28) and i_L can be expressed as:

$$\frac{dv_C}{dt} = v_{Cs}\omega_s \cos(\omega_s t) - v_{Cc}\omega_s \sin(\omega_s t) \tag{30}$$

$$i_L = C\frac{dv_C}{dt} = v_{Cs}C\omega_s \cos(\omega_s t) - v_{Cc}C\omega_s \sin(\omega_s t) \tag{31}$$

It can be easily shown that (25, 26) and (30, 31) are identical expressions. This way, for a series resonant capacitor, the model order residualization technique from control theory is equivalent to the assumption of slowly varying phase and amplitude that is used in the literature to study oscillatory systems and deduce averaged models [1, 22]. The SVAP approach or similar techniques have been applied to mixed systems or converters operating in DCM where one variable can be considered static. Although after applying SVAP/residualization a valid low frequency HBSRI model is obtained [27], it is not formally valid to separate the dynamics of v_c and i_L because a HBSRI is not a mixed system. In order to improve the dynamic results, a SVADP technique is proposed in this paper. Let's consider the amplitude derivative dv_{C1}/dt and phase $\phi(t)$ as slowly varying functions of time. From (1) and after assuming $d^2v_{C1}/dt^2 = 0$, $d\phi/dt = 0$, or $d^2v_{Cc}/dt^2 = 0$, $d^2v_{Cs}/dt^2 = 0$, and applying linearization the following small-signal expressions like (20, 21) are obtained:

$$\begin{pmatrix} d\hat{v}_{Cc}/dt \\ d\hat{v}_{Cs}/dt \end{pmatrix} = \frac{1}{C\Omega_s}\begin{pmatrix} 0 & -1 \\ 1 & 0 \end{pmatrix}\cdot\begin{pmatrix} d\hat{i}_{Lc}/dt \\ d\hat{i}_{Ls}/dt \end{pmatrix} \tag{32}$$

$$\begin{pmatrix} \hat{v}_{Cc} \\ \hat{v}_{Cs} \end{pmatrix} = \frac{1}{C\Omega_s^2}\left[\begin{pmatrix} 0 & -1 \\ 1 & 0 \end{pmatrix}\cdot\begin{pmatrix} \Omega_s\hat{i}_{Lc} + I_{Lc}\hat{\omega}_s \\ \Omega_s\hat{i}_{Ls} + I_{Ls}\hat{\omega}_s \end{pmatrix} + \begin{pmatrix} 1 & 0 \\ 0 & 1 \end{pmatrix}\cdot\begin{pmatrix} d\hat{i}_{Lc}/dt \\ d\hat{i}_{Ls}/dt \end{pmatrix}\right] \tag{33}$$

These expressions allow to reduce the order of the system, (22). The only difference of SVADP from SVAP or residualization would be a zero matrix in (32), and thus the last term of (33) disappears. The small-signal equivalent circuits of the resonant series capacitor after the proposed reduced-order techniques are depicted in Fig. 2. SVAP considers the capacitor as a static element without any dynamic element meanwhile SVADP models its dynamic behavior as an equivalent series inductor. This surprising effect matches perfectly with the simplified equivalent circuit for a SRC proposed in [11]. After substituting (33) in (15), the 4th small-signal model can be rewritten as a 2nd reduced-order one as:

$$\frac{d}{dt}\hat{\mathbf{x}}_r = \mathbf{A}_r\hat{\mathbf{x}}_r + \mathbf{B}_{\omega r}\hat{\omega}_S + \mathbf{B}_{dr}\hat{d} \tag{34}$$

where

$$\hat{\mathbf{x}}_r = \begin{pmatrix} \hat{i}_{Lc} & \hat{i}_{Ls} \end{pmatrix}^T \tag{35}$$

$$\mathbf{A}_r = \begin{pmatrix} -R/L_e & -X/L_e \\ X/L_e & -R/L_e \end{pmatrix} \tag{36}$$

$$\mathbf{B}_{\omega r} = \begin{pmatrix} -I_{Ls} \\ I_{Lc} \end{pmatrix}, \quad \mathbf{B}_{dr} = \frac{2V_g}{L_e}\begin{pmatrix} \cos(2\pi D) \\ \sin(2\pi D) \end{pmatrix} \tag{37}$$

$$L_e = L + 1/(C\Omega_s^2)) = L(1 + 1/\Omega_n^2) \tag{38}$$

$$\Omega_n = \Omega_s/\Omega_0, \quad \Omega_0 = 1/\sqrt{LC} \tag{39}$$

The complete small signal equivalent circuits of EDF and SVADP are depicted in Fig.3. The SVAP small-signal equivalent circuit would be exactly equal to the one from SVADP except for substituting L_e by L.

B. Small signal, low frequency current and power models

Once the reduced-order model has been obtained with SVADP approach, a second order model of the current phase angle θ, current amplitude i_{L1} and power P transfer functions respect d and ω_{sw} will be obtained analytically. Let φ be the phase angle of the inverter voltage, thus, equations (2) and (4) can be rearranged as follows:

$$i_L(t) = i_{L1}(t)\sin(\omega_s t + \theta) \tag{40}$$

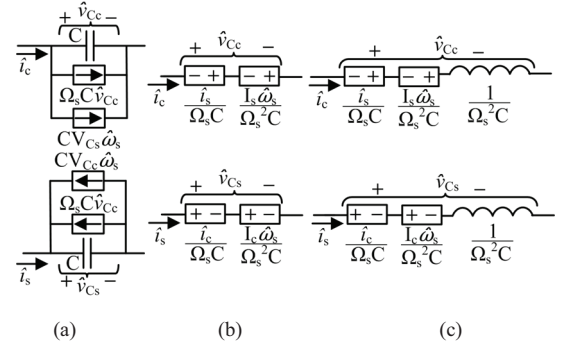$$u(t) = u_0 + u_1(t)\sin(\omega_s t + \varphi) \tag{41}$$

Fig. 2. Equivalent small signal circuit for a series capacitor (a) EDF, (b) SVAP/residualization and (c) SVADP.
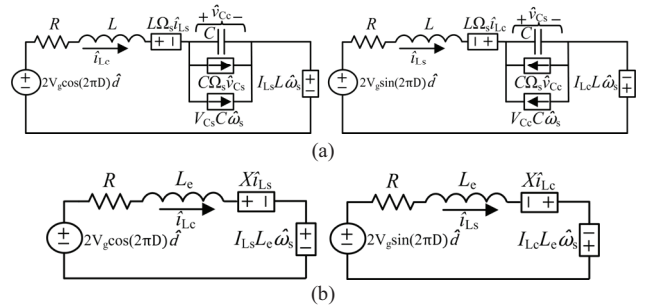

Fig. 3. Equivalent small signal circuit for a HBSRI for Spice Simulation obtained by (a) EDF and (b) SVADP.

The relation between the current amplitude i_L and the current phase angle θ to the control inputs, d and ω_{sw}, is nonlinear, and small-signal analysis was employed in [18, 19]. The small signal duty-to-phase-angle θ, $G_{\theta d}(s)$, angular frequency-to-phase-angle, $G_{\theta\omega}(s)$, duty-to-output-power, $G_{pd}(s)$, and angular frequency-to-output-power, $G_{p\omega}(s)$, transfer functions are used in [19] to implement a multi-loop power control loop, but no analytical expressions were given. In order to obtain the small-signal transfer functions we linearize the output equations. The current phase angle, amplitude current and power output equations are:

$$\theta = h_1(\mathbf{x}) = tg^{-1}\left(\frac{i_{Lc}}{i_{Ls}}\right) \tag{42}$$

$$i_L = h_2(\mathbf{x}) = \sqrt{i_{Lc}^2 + i_{Ls}^2} \tag{43}$$

$$P = h_3(\mathbf{x}) = \frac{1}{2}R\left(i_{Lc}^2 + i_{Ls}^2\right) \tag{44}$$

The linearized output equations near $\mathbf{x}_e$ are obtained as:

$$\hat{\theta} = \mathbf{C_\theta}\hat{\mathbf{x}}, \quad \hat{i} = \mathbf{C_i}\hat{\mathbf{x}}, \quad \hat{p} = \mathbf{C_p}\hat{\mathbf{x}} \tag{45}$$

where

$$\mathbf{C_\theta} = \left.\frac{\partial h_1}{\partial \mathbf{x}}\right|_{\mathbf{x}_e} = \frac{1}{I_{Lc}^2 + I_{Ls}^2}\left(I_{Ls} \quad -I_{Lc}\right) \tag{46}$$

$$\mathbf{C_i} = \left.\frac{\partial h_2}{\partial \mathbf{x}}\right|_{\mathbf{x}_e} = \frac{1}{\sqrt{I_{Lc}^2 + I_{Ls}^2}}\left(I_{Lc} \quad I_{Ls}\right) \tag{47}$$

$$\mathbf{C_p} = \left.\frac{\partial h_3(\mathbf{x})}{\partial \mathbf{x}}\right|_{\mathbf{x}_e} = R\left(I_{Lc} \quad I_{Ls}\right) \tag{48}$$

The second order transfer functions reflected in the appendix A. The output power in the steady-state operating point P_e is calculated by substituting (11) in (44):

$$P_e = \frac{1}{2}R\left(I_{Lc}^2 + I_{Ls}^2\right) = 2\left(\frac{V_g}{\pi}\right)^2 \frac{R\sin^2(\pi D)}{Z^2} \tag{49}$$

For a better understanding of the proposed reduced order model, let's compare the poles location with the ones from original EDF model. The expression of the low frequency complex-conjugate poles pair of the 4th order EDF model under high Q assumption [15], and the ones from SVAP and SVADP are:

$$p_{1,2_{EDF}} = -\frac{R}{2L} \pm j\Omega_s\left(1 - \frac{1}{\Omega_n}\right) \tag{50}$$

$$p_{1,2_{SVAP}} = -\frac{R}{L} \pm j\Omega_s\left(1 - \frac{1}{\Omega_n}\right)\left(1 + \frac{1}{\Omega_n}\right) \tag{51}$$

$$p_{1,2_{SVADP}} = -\frac{R}{L\left(1 + \frac{1}{\Omega_n^2}\right)} \pm j\Omega_s\left(1 - \frac{1}{\Omega_n}\right)\frac{\left(1 + \frac{1}{\Omega_n}\right)}{\left(1 + \frac{1}{\Omega_n^2}\right)} \tag{52}$$

It can be seen that SVADP estimates both real and imaginary parts of complex-conjugate poles better than SVAP. This will lead to better dynamic results. SVADP poles location estimation improves more and more when Ω_s is near Ω_0 predicting exactly its location at resonance ($\Omega_n=1$). Regarding the zeroes, an important effect is present in the zero location of $G_{idr}(s)$ (A2) and $G_{idr}(s)$ (A3). The expression of this zero is:

$$z = -\frac{Z}{L_e}\frac{Z}{R + X\tan(\pi D)} \tag{53}$$

This zero location is mainly determined by D. Its influence respect the complex-conjugate poles location will become important when both frequencies start to be similar. For the usual operating mode, $D \leq 0.5$, its influence will be noticeable when (53) is comparable to or smaller than the natural frequency of (52), i.e. when D will be in this interval:

$$\pi^{-1}\tan^{-1}\left(\frac{Z-R}{X}\right) \leq D \leq 0.5 \tag{54}$$

Fig.4 depicts the relationship of this zero respect the natural frequency of the poles of the SVADP reduced-order model for $\Omega_n=1.5$. It can be seen that the zero is at the origin at exactly D=0.5. This effect is also present in the EDF original model and it is a consequence of the maximum that occurs at that point. A similar effect can be seen for $G_{p\omega}(s)$ when the switching frequency is exactly the resonant one. Since there is also a maximum in this case, the steady-state gain drops to zero as reported in [11].

In [29], the transfer function from the inverter voltage phase φ to the current phase angle θ is reported as a first-order system under resonance operation $\Omega_n=1$. Considering this premise, the following transfer function is obtained from SVADP reduced-order model:
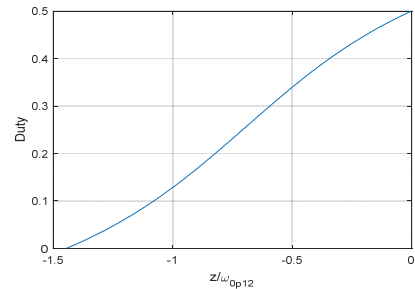

Fig. 4. Relationship of the $G_{pd}(s)$ and $G_{pi}(s)$ zero respect the natural frequency of the complex conjugate poles for $\Omega_n=1.5$ and D<=0.5.

$$G_{\theta\varphi r} = \frac{G_{\theta dr}}{\partial \varphi / \partial d} = \frac{G_{\theta dr}}{-\pi} = \frac{1}{\left(1 + sL_e / R\right)} \qquad (55)$$

The value of $\partial\varphi / \partial d$ is derived in [18]. Under resonance operation, a zero-pole cancellation occurs in $G_{\theta dr}(s)$ (A1) and thus a first-order transfer function is obtained in (55). This zero-pole cancellation also occurs in $G_{\theta\omega r}(s)$ (A1), which means that under resonance operation θ behaves as a first-order response. Although the time constant is L_e/R in (55) and $2L/R$ in [29], under resonance operation $L_e=2L$ (38). Thus SVADP model provides identical results as [29].

III. HBSRI MODEL REDUCTION WITH SVADP METHOD

A. DHBSRI SVADP model order reduction

Although, the SVADP order reduction technique has been shown for a simple HBSRI, it can also be applied to multivariable plants with a greater order. In this section, the reduction technique will be applied to a DHBSRI sharing resonant capacitor. Phase Shift Square Wave Modulation with $D = 0.5$ is considered to control the output power of both loads (Fig. 5). This system has three state variables, and the EDF modeling method will get transfer functions of sixth order [16]. Thus, in this section, it will be derived a 4th and a 2nd order approximation of the transfer functions by applying the SVADP reduced order technique.

From the large signal model [16] and considering the amplitude derivative dv_{C1}/dt and phase $\phi(t)$ of the shared resonant capacitor as slowly varying functions of time ($d^2 v_{Cc}/dt^2 = 0$, $d^2 v_{Cs}/dt^2 = 0$), similar expressions to (32, 33) are obtained as:

$$\begin{pmatrix} d\hat{v}_{Cc}/dt \\ d\hat{v}_{Cs}/dt \end{pmatrix} = \frac{1}{C\omega_s} \begin{pmatrix} 0 & -1 & 0 & -1 \\ 1 & 0 & 1 & 0 \end{pmatrix} \cdot \begin{pmatrix} d\hat{i}_{Lc1}/dt \\ d\hat{i}_{Ls1}/dt \\ d\hat{i}_{Lc2}/dt \\ d\hat{i}_{Ls2}/dt \end{pmatrix} \qquad (56)$$

$$\begin{pmatrix} \hat{v}_{Cc} \\ \hat{v}_{Cs} \end{pmatrix} = \frac{1}{C\Omega_s^2} \begin{bmatrix} \begin{pmatrix} 0 & -1 \\ 1 & 0 \end{pmatrix} \cdot \begin{pmatrix} \Omega_s(\hat{i}_{Lc1}+\hat{i}_{Lc2})+(I_{Lc1}+I_{Lc2})\hat{\omega}_s \\ \Omega_s(\hat{i}_{Ls1}+\hat{i}_{Ls2})+(I_{Ls1}+I_{Ls2})\hat{\omega}_s \end{pmatrix} + \\ \begin{pmatrix} 1 & 0 & 1 & 0 \\ 0 & 1 & 0 & 1 \end{pmatrix} \cdot \begin{pmatrix} d\hat{i}_{Lc1}/dt \\ d\hat{i}_{Ls1}/dt \\ d\hat{i}_{Lc2}/dt \\ d\hat{i}_{Ls2}/dt \end{pmatrix} \end{bmatrix} \qquad (57)$$

These expressions allow to reduce the order of the system from a 6th order model to a 4th order one. The only difference of SVADP from SVAP or residualization would be a zero matrix in (56), and thus the last term of (57) disappears.
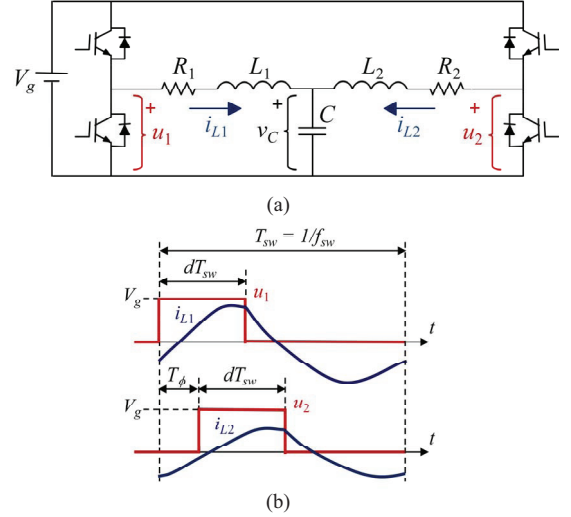
(a)

(b)

Fig. 5. DHBSRI sharing resonant capacitor (a) schematic (b) main waveforms

When substituting (57) in the EDF small-signal model, some algebra manipulation is required to obtain the reduced 4th order model because both $\hat{v}_{Cc}$ and $\hat{v}_{Cs}$ in (57) depends on two different dynamic terms. This will make more difficult to obtain analytical expressions compared to the HBSRI, apart from the higher order. The 6th order EDF small-signal model [16] can be reduced as a 4th order one as:

$$\frac{d}{dt}\hat{\mathbf{x}}_r = \mathbf{A}_r \hat{\mathbf{x}}_r + \mathbf{B}_{\omega r}\hat{\omega}_s + \mathbf{B}_{\phi r}\hat{\phi} \qquad (58)$$

where

$$\hat{\mathbf{x}}_r = \begin{pmatrix} \hat{i}_{Lc1} & \hat{i}_{Ls1} & \hat{i}_{Lc2} & \hat{i}_{Ls2} \end{pmatrix}^T \qquad (59)$$

$$\mathbf{A}_r = \begin{pmatrix} -R_1/L_{1e} & -X_{1e}/L_{1e} & R_{2c}/L_{1e} & X_{2c}/L_{1e} \\ X_{1e}/L_{1e} & -R_1/L_{1e} & -X_{2c}/L_{1e} & R_{2c}/L_{1e} \\ R_{1c}/L_{2e} & X_{1c}/L_{2e} & -R_2/L_{2e} & -X_{2e}/L_{2e} \\ -X_{1c}/L_{2e} & R_{1c}/L_{2e} & X_{2e}/L_{2e} & -R_2/L_{2e} \end{pmatrix} \qquad (60)$$

$$\mathbf{B}_{\omega r} = \begin{pmatrix} -I_{Ls1} & I_{Lc1} & -I_{Ls2} & I_{Lc2} \end{pmatrix}^T \qquad (61)$$

$$\mathbf{B}_{\phi r} = \frac{2V_g}{\pi} \begin{pmatrix} \cos(\Phi)/L_{e1\phi} \\ \sin(\Phi)/L_{e1\phi} \\ -\cos(\Phi)/L_{e2\phi} \\ -\sin(\Phi)/L_{e2\phi} \end{pmatrix} \qquad (62)$$

Where

$$\Omega_{0_1} = 1/\sqrt{L_1 C}, \quad \Omega_{0_2} = 1/\sqrt{L_2 C} \qquad (63)$$

$$\Omega_{n_1} = \Omega_s/\Omega_{0_1}, \quad \Omega_{n_2} = \Omega_s/\Omega_{0_2} \qquad (64)$$

$$L_{1e} = L_1(1 + \frac{\Omega_{n_2}^2}{\Omega_{n_1}^2(1+\Omega_{n_2}^2)}), \quad L_{2e} = L_2(1 + \frac{\Omega_{n_1}^2}{\Omega_{n2}^2(1+\Omega_{n_1}^2)}) \quad (65)$$

$$X_{1e} = L_1\Omega_s(1 - \frac{\Omega_{n_2}^2}{\Omega_{n_1}^2(1+\Omega_{n_2}^2)}), \quad X_{2e} = L_2\Omega_s(1 - \frac{\Omega_{n_1}^2}{\Omega_{n_2}^2(1+\Omega_{n_1}^2)}) \quad (66)$$

$$R_{1c} = \frac{R_1}{1+\Omega_{n_1}^2}, \quad R_{2c} = \frac{R_2}{1+\Omega_{n_2}^2} \quad (67)$$

$$X_{1c} = \frac{2L_1\Omega_s}{1+\Omega_{n_1}^2}, \quad X_{2c} = \frac{2L_2\Omega_s}{1+\Omega_{n_2}^2} \quad (68)$$

$$L_{e1\phi} = L_1 + L_2(1+\Omega_{n_1}^2), \quad L_{e2\phi} = L_2 + L_1(1+\Omega_{n_1}^2)^{-1} \quad (69)$$

It can be observed that after SVADP reduction technique applied to the shared resonant capacitor; there are important interactions between every state variable since there are no zero elements in the reduced state matrix $\mathbf{A_r}$. A similar dynamic effect as in HBSRI can be observed in the equivalent inductances L_{1e}, L_{2e}, and reactances X_{1e}, X_{2e}, except for the interaction of the other individual resonant frequency. The small-signal equivalent circuit of the EDF and the SVADP reduced-models are depicted in Fig. 6.

Although a 2nd order reduction from a 6th order model is quite helpful, the analytical expressions to be obtained require inverting a 4x4 $\mathbf{A_r}$ matrix being a bit cumbersome. When analyzing the reduced-order model (58) and the equivalent circuit in Fig. 6, there is a clear coupling between both current branches. If that coupling could be removed, a simple 2nd order transfer function would be obtained. In order to provide simpler analytical expressions, a further reduced-order model of 2nd order is proposed. Although SVADP approach has only been applied in previous sections to the series resonant capacitor voltage, the same technique can be perfectly applied to other state variables.

Let's consider every time derivative of (59) as slowly varying functions of time. Thus, considering null every second derivative of (59), the following expressions from (58) are obtained:

$$\begin{pmatrix} d\hat{i}_{Lck}/dt \\ d\hat{i}_{Lsk}/dt \end{pmatrix} = \begin{pmatrix} R_k & X_{ke} \\ -X_{ke} & R_k \end{pmatrix}^{-1} \begin{pmatrix} R_{lc} & X_{lc} \\ -X_{lc} & R_{lc} \end{pmatrix} \begin{pmatrix} d\hat{i}_{Lcl}/dt \\ d\hat{i}_{Lsl}/dt \end{pmatrix} \quad (70)$$

$$\begin{pmatrix} \hat{i}_{Lck} \\ \hat{i}_{Lsk} \end{pmatrix} = \begin{pmatrix} R_k & X_{ke} \\ -X_{ke} & R_k \end{pmatrix}^{-1} \begin{bmatrix} -\begin{pmatrix} R_{lc} & X_{lc} \\ -X_{lc} & R_{lc} \end{pmatrix} \cdot \begin{pmatrix} \hat{i}_{Lcl} \\ \hat{i}_{Lsl} \end{pmatrix} - \begin{pmatrix} -I_{Lsk} \\ I_{Lck} \end{pmatrix} + \\ (-1)^k \frac{2V_gL_{ke}}{\pi L_{ek\phi}} \begin{pmatrix} \cos(\Phi) \\ \sin(\Phi) \end{pmatrix} - \\ L_{ke}\begin{pmatrix} R_k & X_{ke} \\ -X_{ke} & R_k \end{pmatrix}^{-1} \begin{pmatrix} R_{lc} & X_{lc} \\ -X_{lc} & R_{lc} \end{pmatrix} \begin{pmatrix} d\hat{i}_{Lcl}/dt \\ d\hat{i}_{Lsl}/dt \end{pmatrix} \end{bmatrix} \quad (71)$$

Where subscript k makes reference to the considered k output and its parameters meanwhile subscript l makes reference to the other coupled l current branch and its parameters. The only difference of SVADP from SVAP or residualization would be a zero matrix in (70), and thus the last term of (71) disappears. After substituting (71) in the reduced 4th order model (58) and after some algebra manipulation the following 2nd reduced-order model is obtained as follows:

$$\frac{d}{dt}\hat{\mathbf{x}}_{r2_k} = \mathbf{A}_{r2_k}\hat{\mathbf{x}}_{r2_k} + \mathbf{B}_{\omega r2_k}\hat{\omega}_s + \mathbf{B}_{\phi r2_k}\hat{\phi} \quad (72)$$

where

$$\mathbf{x}_{r2_k} = \begin{pmatrix} \hat{i}_{Lck} & \hat{i}_{Lsk} \end{pmatrix}^T \quad (73)$$

$$\mathbf{A}_{r2_k} = \begin{pmatrix} -R'_{ke}/L'_{ke} & -X'_{ke}/L'_{ke} \\ X'_{ke}/L'_{ke} & -R'_{ke}/L'_{ke} \end{pmatrix} \quad (74)$$

$$\mathbf{B}_{\omega r2_k} = \frac{1}{L'_{ke}}\begin{pmatrix} -I'_{Lsk} \\ I'_{Lck} \end{pmatrix}, \quad \mathbf{B}_{\phi r2_k} = \frac{2V_g}{\pi L'_{ke}}\begin{pmatrix} K_{\phi 1k} \\ K_{\phi 2k} \end{pmatrix} \quad (75)$$

The small-signal equivalent circuit of the SVADP reduced-models of 2nd order is depicted in Fig. 7.

B. Small signal, low frequency current and power models

The considered output variables are the angle currents, θ_1, θ_2, the currents i_{L1}, i_{L2} and the output powers P_1, P_2, as in previous section. The control variables are now the switching frequency ω_S and the phase delay ϕ given by:

$$\phi = 2\pi T_\phi / T_S \quad (76)$$

where T_ϕ is the delay between the two excitation voltages shown in Fig.5.

As in previous section, the linearized output equations near $\mathbf{x}_e$ for k output are obtained as:

$$\hat{\theta}_k = \mathbf{C}_{\theta_k}\hat{\mathbf{x}}, \quad \hat{i}_k = \mathbf{C}_{i_k}\hat{\mathbf{x}}, \quad \hat{p}_k = \mathbf{C}_{p_k}\hat{\mathbf{x}} \quad (77)$$

where

$$\mathbf{C}_{\theta_k} = \frac{1}{I_{Lck}^2 + I_{Lsk}^2}(I_{Lsk} \quad -I_{Lck}) \quad (78)$$

$$\mathbf{C}_{i_k} = \frac{1}{\sqrt{I_{Lck}^2 + I_{Lsk}^2}}(I_{Lck} \quad I_{Lsk}) \quad (79)$$

$$\mathbf{C}_{p_k} = R_k(I_{Lck} \quad I_{Lsk}) \quad (80)$$

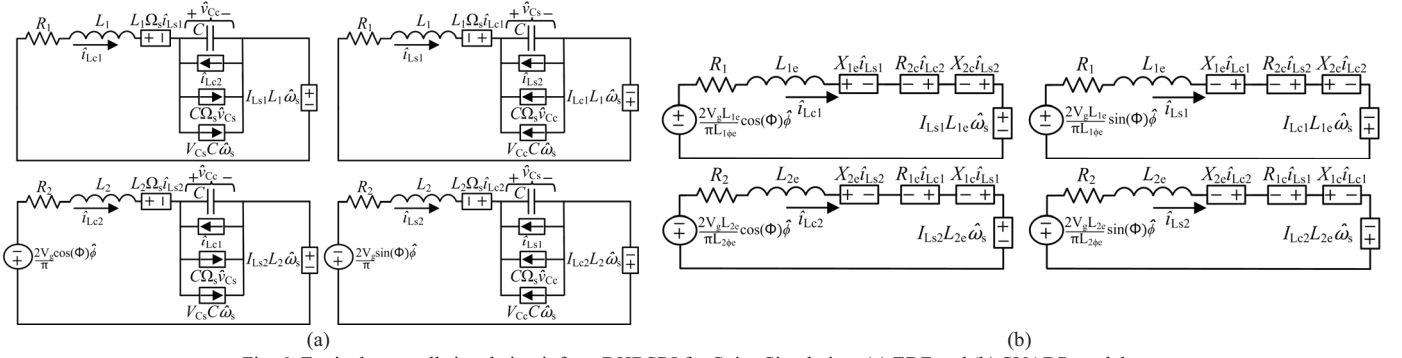The second order transfer functions are reflected in Appendix A.

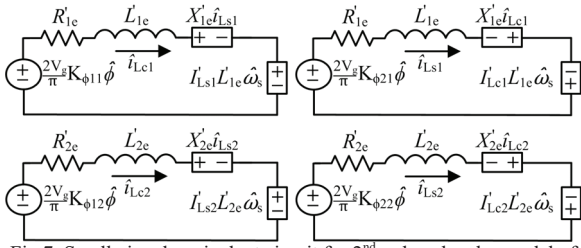Fig. 6. Equivalent small signal circuit for a DHBSRI for Spice Simulation. (a) EDF and (b) SVADP models.

Fig.7. Small-signal equivalent circuit for 2nd reduced-order model of DHBSRI from SVADP.

$$\left\| G_{pd} \right\|_\infty = \sup_\omega \left\| G_{pd} \right\|^{-1} \left(\left| G_{pd} \right| - \left| G_{pdr} \right| \right),$$
$$\angle G_{pd\infty} = \sup_\omega \left| \angle G_{pd} - \angle G_{pdr} \right| \tag{82}$$

$$\left\| G_{p\omega} \right\|_\infty = \sup_\omega \left\| G_{p\omega} \right\|^{-1} \left(\left| G_{p\omega} \right| - \left| G_{p\omega r} \right| \right),$$
$$\angle G_{p\omega\infty} = \sup_\omega \left| \angle G_{p\omega} - \angle G_{p\omega r} \right| \tag{83}$$

IV. SIMULATION AND EXPERIMENTAL RESULTS

Some simulation and experimental results are shown in this section to validate the reduction order technique. Most of the results have been obtained by using a normalized induction heating load with the following values: resistance $R = 2.9\ \Omega$; inductance $L = 19\ \mu H$; resonant capacitor $C = 1.44\ \mu F$. The resulting resonant frequency and quality factor are $f_0 = 30.4$ kHz and Q = 1.25. The input bus voltage is $V_g = 230$ V. In the case of the dual half-bridge topology, the second load was a conventional induction cooking pot characterized by $R = 5.9\ \Omega$ and $L = 39\ \mu H$.

Fig. 8 shows the Bode plots of the small signal transfer functions developed in Section II with $\omega_s = 1.1\omega_0$ and $D = 0.4$. The last subscript in the legends represents: without subscript, the reference 4th order system; r, the SVADP reduced 2nd order system; r0, the SVAP reduced 2nd order system. A normalized angular frequency ω_n is used in the frequency axis:

$$\omega_n = \omega_s / \omega_0 \tag{81}$$

The frequency range is extended from 0.01 ω_0 to 0.5ω_0. A good agreement up to frequencies about one tenth of the resonant frequency is obtained, especially with the SVADP reduction technique, which matches the reference system better than the SVAP approximation.

In order to measure the distance between the reduced-order systems and the 4th order one, the H_∞ relative norm and the maximum phase error of the transfer functions can be computed in the frequency range of interest. Fig.9 shows these metrics for the duty-to-output power, $G_{pd}(s)$, and angular frequency-to-output power, $G_{p\omega}(s)$, transfer functions. The magnitudes shown are defined as follow:

The frequency range extends up to $\omega_0/5$ in Fig. 9. In these figures, a parameter range of $1.1 \le \omega_n \le 3.3$, $0.1 \le D \le 0.4$, and $1.0 \le Q \le 5.0$ is considered. One of the parameters is modified in its range while the others are kept constant to the default values of $\omega_n = 1.5$, $D = 0.4$, and $Q = 1.5$. From this figure it can be stated that the magnitude worst-case error is below 7 % for both power transfer functions. When D approaches 0.5, the duty-to-output power transfer function error increases. This is explained because $G_{pd}(s)$ has a singularity in $D = 0.5$, where the phase has a sharp change of 180º as explained in section II. The maximum phase error is below 4º except for the angular power transfer function, whose phase error rises up to 18º close to resonance.

The maximum frequency considered is of vital importance. In the worst case, a maximum H_∞ relative norm of 7 % is obtained for $\omega_0/5$ and 3 % for $\omega_0/10$. The same applies to the phase error. In the domestic induction appliances field, where Q is approximately constant with values about 1.5, the worst case phase error is 3º for $\omega_0/5$ and 1º for $\omega_0/10$.

Fig. 10 shows the Bode plots of the small signal output power transfer functions of the DHBSRI developed in Section III. The legends represent: without subscript, the complete 6th order system; 4, the reduced 4th order system; 2 the reduced 2nd order system. The simulation parameters are $f_{sw} = 38$ kHz (corresponding to $1.25\Omega_{01}$, $D = 0.5$, and $\phi = 90º$. In these conditions, the steady-state output power is 3600 W for the first load and 165 W for the second one. A close agreement between the reference and the 4th order reduced system can be observed in all the frequency range, up to half Ω_{01}. The 2nd order approximation shows more error as expected, especially when frequency increases.
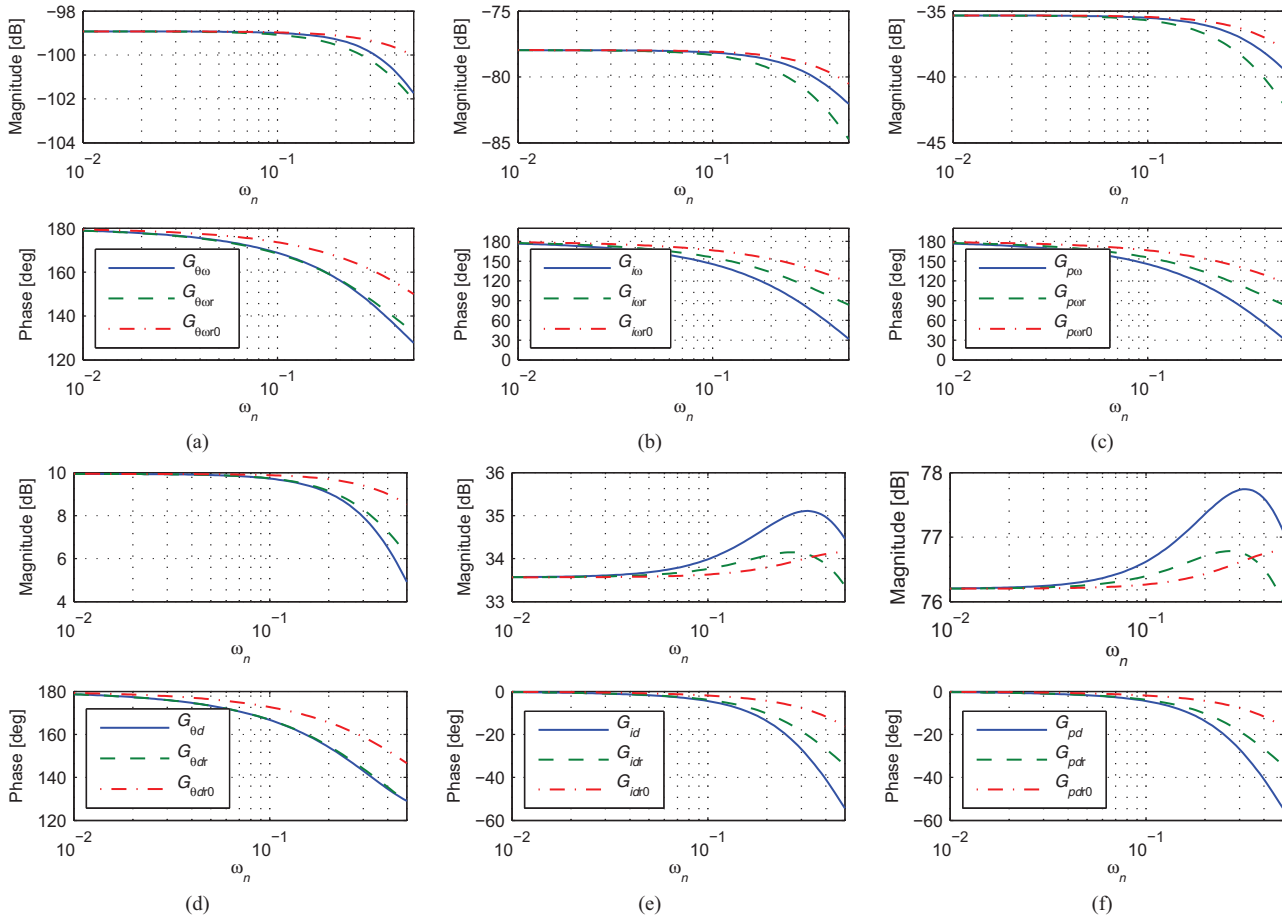
Fig. 8. Comparative of transfer functions for the 2nd order system with $\omega_s = 1.1\omega_0$ and $D = 0.4$. The last subscript in the legends represents: without subscript, the complete 4th order system; r, the SVADP reduced 2nd order system; r0, the SVAP 2nd order approximation.
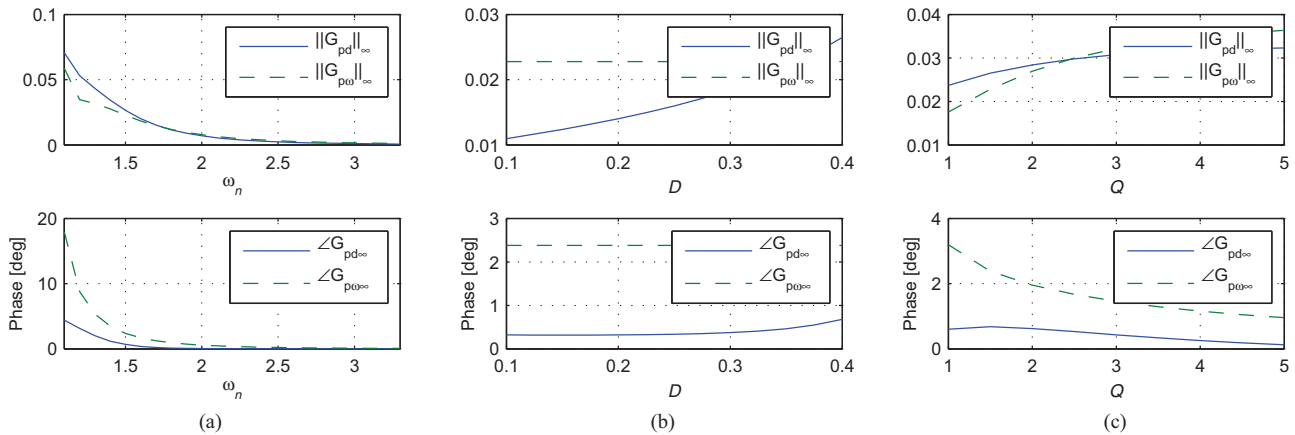

Fig. 9. H$_\infty$ relative norm and maximum phase error of the SVADP 2nd order approximation respect to the 4th order power transfer functions varying (a) ω_n, (b) D, and (c) Q. The default parameters are $\omega_n = 1.5$, $D = 0.4$, $Q = 1.5$. The maximum angular frequency is $\omega_0/5$

Some experimental results have been conducted in order to measure the real transfer function and compare it with the obtained reduced order models. The experimental tests have been conducted in the worst scenario in order to verify adequately the validity range. Fig. 11 shows the Bode plot of the duty-to output power $G_{pd}(s)$ and frequency-to output power $G_{pf}(s)$ obtained for a half-bridge series resonant inverter for the operating point (f_{sw}, D) = (42 kHz, 0.45). Fig. 12 shows the test bed for conducting the experimental results.

Despite a commercial vessel has been considered and the operating point is far from resonance and near the singularity point of $D = 0.5$, a very good agreement up to frequencies about one tenth of the switching frequency is obtained. It can be observed that $G_{pd}(s)$ magnitude increases with the frequency due to the location of the transfer function zero nearer to the origin than the complex-conjugate poles with this load and operation point.
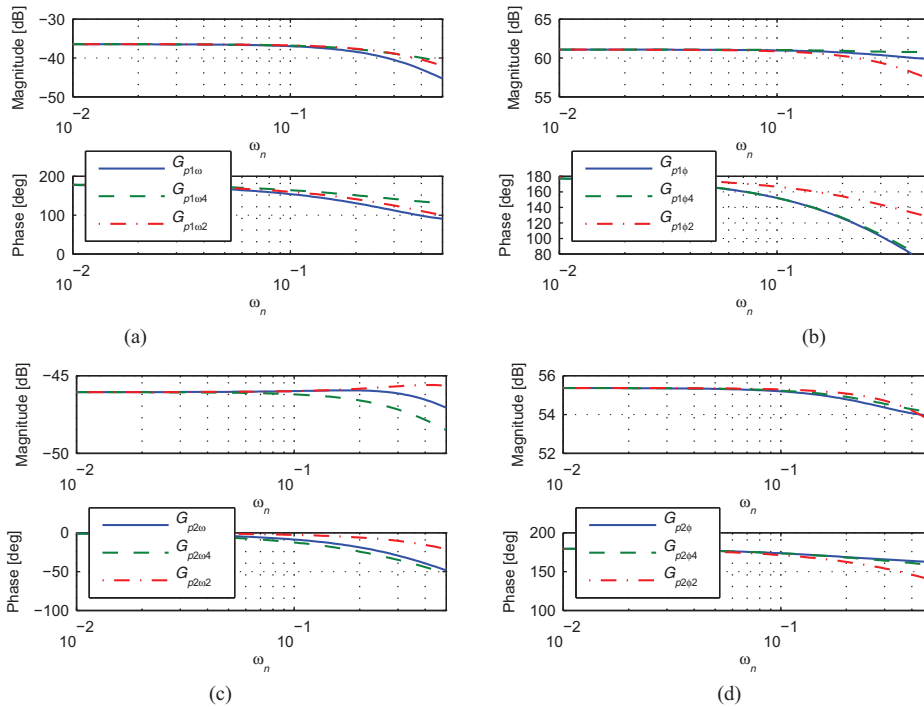
Fig. 10. Comparative of the output power Bode plots for the DHBSRI with ω_s=1.1ω_0, D=0.5, and ϕ=90º, (a) and (b) first load, (c) and (d) second load. The last subscript in the legends represents: without subscript, the complete 6th order system; 4, the reduced 4th order system; 2 the 2nd order system.
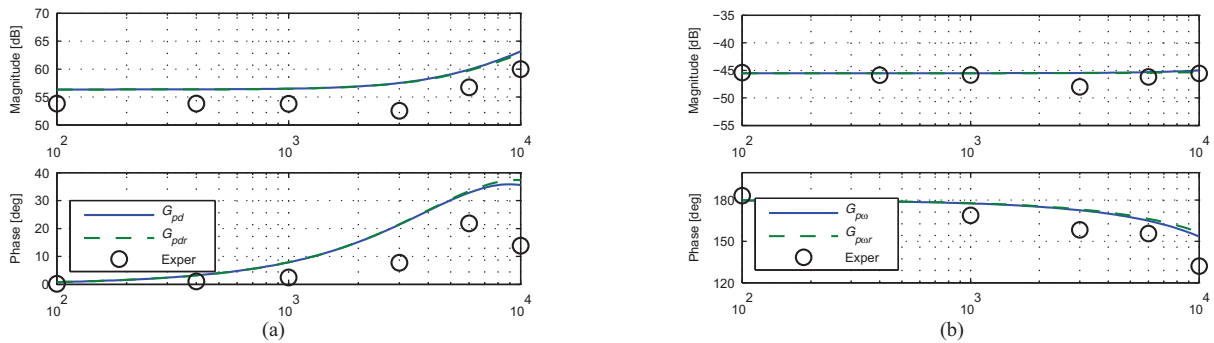
Fig. 11. Comparative of experimental results and proposed reduced-order models for f_{sw}=42 kHz, D=0.45 (a) $G_{pd}(s)$ and (b) $G_{pf}(s)$. Frequency in Hz is shown in the horizontal axis.

Fig. 12. Experimental induction heating prototype.

APPENDIX A

The second order transfer functions from SVADP reduced order technique for the HBSRI are the following:

$$G_{\theta\omega r} = -\frac{s+R/L_e}{\left(s+R/L_e\right)^2+\left(X/L_e\right)^2}, \quad G_{\theta dr} = \frac{\pi}{L_e}\left(\frac{X}{\tan(\pi D)}-R\right)\frac{s+Z/L_e\left(Z/(R-X/\tan(\pi D))\right)}{\left(s+R/L_e\right)^2+\left(X/L_e\right)^2} \quad (A1)$$

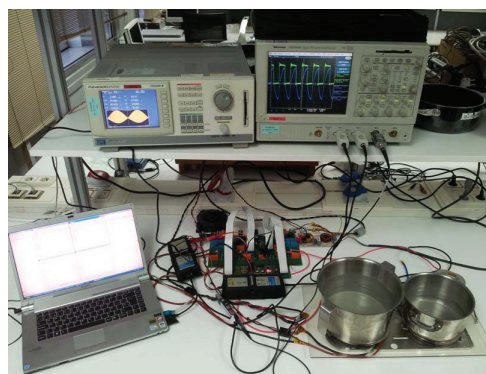$$G_{i\omega r} = -\frac{2V_gX}{\pi L_eZ}\frac{\sin(\pi D)}{\left(s+R/L_e\right)^2+\left(X/L_e\right)^2}, \quad G_{idr} = \frac{2V_g}{L_eZ}\left(\frac{R}{\tan(\pi D)}+X\right)\frac{s+Z/L_e\left(Z/(R+X\tan(\pi D))\right)}{\left(s+R/L_e\right)^2+\left(X/L_e\right)^2} \quad (A2)$$

$$G_{p\omega r} = -\frac{2XP_e}{L_e}\frac{1}{\left(s+R/L_e\right)^2+\left(X/L_e\right)^2}, \quad G_{pdr} = \frac{2\pi P_e}{L_e}\left(\frac{R}{\tan(\pi D)}+X\right)\frac{s+Z/L_e\left(Z/(R+X\tan(\pi D))\right)}{\left(s+R/L_e\right)^2+\left(X/L_e\right)^2} \quad (A3)$$

For the DHBSRI, the second order transfer functions from SVADP reduced order technique are the following:

$$G_{\theta\omega r2_k} = -\frac{(I_{Lsk}I'_{Lsk}+I_{Lck}I'_{Lck})(s+R'_{ke}/L'_{ke})+(I_{Lsk}I'_{Lck}-I_{Lck}I'_{Lsk})X'_{ke}/L'_{ke}}{L'_{ke}(I_{Lck}{}^2+I_{Lsk}{}^2)\left(\left(s+R'_{ke}/L'_{ke}\right)^2+\left(X'_{ke}/L'_{ke}\right)^2\right)} \quad (A4)$$

$$G_{\theta\phi r2_k} = -\frac{2V_g}{\pi L'_{ke}}\frac{(-I_{Lsk}K_{\phi1k}+I_{Lck}K_{\phi2k})(s+R'_{ke}/L'_{ke})+(I_{Lsk}K_{\phi2k}+I_{Lck}K_{\phi1k})X'_{ke}/L'_{ke}}{(I_{Lck}{}^2+I_{Lsk}{}^2)\left(\left(s+R'_{ke}/L'_{ke}\right)^2+\left(X'_{ke}/L'_{ke}\right)^2\right)} \quad (A5)$$

$$G_{i\omega r2_k} = -\frac{(I_{Lck}I'_{Lsk}-I_{Lsk}I'_{Lck})(s+R'_{ke}/L'_{ke})+(I_{Lck}I'_{Lck}+I_{Lsk}I'_{Lsk})X'_{ke}/L'_{ke}}{L'_{ke}\sqrt{I_{Lck}^2+I_{Lsk}^2}\left(\left(s+R'_{ke}/L'_{ke}\right)^2+\left(X'_{ke}/L'_{ke}\right)^2\right)} \quad (A6)$$

$$G_{i\phi r2_k} = -\frac{2V_g}{\pi L'_{ke}}\frac{(-I_{Lck}K_{\phi1k}-I_{Lsk}K_{\phi2k})(s+R'_{ke}/L'_{ke})+(I_{Lck}K_{\phi2k}-I_{Lsk}K_{\phi1k})X'_{ke}/L'_{ke}}{\sqrt{I_{Lck}^2+I_{Lsk}^2}\left(\left(s+R'_{ke}/L'_{ke}\right)^2+\left(X'_{ke}/L'_{ke}\right)^2\right)} \quad (A7)$$

$$G_{p\omega r2_k} = -R_k\frac{(I_{Lck}I'_{Lsk}-I_{Lsk}I'_{Lck})(s+R'_{ke}/L'_{ke})+(I_{Lck}I'_{Lck}+I_{Lsk}I'_{Lsk})X'_{ke}/L'_{ke}}{L'_{ke}\left(\left(s+R'_{ke}/L'_{ke}\right)^2+\left(X'_{ke}/L'_{ke}\right)^2\right)} \quad (A8)$$

$$G_{p\phi r2_k} = -\frac{2V_gR_k}{\pi L'_{ke}}\frac{(-I_{Lck}K_{\phi1k}-I_{Lsk}K_{\phi2k})(s+R'_{ke}/L'_{ke})+(I_{Lck}K_{\phi2k}-I_{Lsk}K_{\phi1k})X'_{ke}/L'_{ke}}{\left(s+R'_{ke}/L'_{ke}\right)^2+\left(X'_{ke}/L'_{ke}\right)^2} \quad (A9)$$

Where

$$R'_{ke} = R_k - \frac{R_{lc}(R_lR_{kc}+X_{le}X_{kc})-X_{lc}(R_lX_{kc}-X_{le}R_{kc})}{R_l{}^2+X_{le}{}^2} \quad (A10)$$

$$X'_{ke} = X_{ke} - \frac{R_{lc}(R_lX_{kc}-X_{le}R_{kc})+X_{lc}(R_lR_{kc}+X_{le}X_{kc})}{R_l{}^2+X_{le}{}^2} \quad (A11)$$

$$L'_{ke} = L_{ke} + L_{le}\left(\frac{R_lR_{lc}+X_{le}X_{lc}}{R_l{}^2+X_{le}{}^2}\beta_{1k}+\frac{X_{lc}R_l-R_{lc}X_{le}}{R_l{}^2+X_{le}{}^2}\beta_{2k}\right) \quad (A12)$$

$$I'_{\text{Lsk}} = L_{\text{ke}}I_{\text{Lsk}} + \frac{L_{\text{le}}I_{\text{Lsl}}(R_{\text{lc}}R_{\text{l}} + X_{\text{lc}}X_{\text{le}}) + L_{\text{le}}I_{\text{Lcl}}(R_{\text{lc}}X_{\text{le}} - X_{\text{lc}}R_{\text{l}})}{R_{\text{l}}{}^2 + X_{\text{le}}{}^2} \quad \text{(A13)}$$

$$I'_{\text{Lck}} = L_{\text{ke}}I_{\text{Lck}} + \frac{-L_{\text{le}}I_{\text{Lsl}}(R_{\text{lc}}X_{\text{le}} - X_{\text{lc}}R_{\text{l}}) + L_{\text{le}}I_{\text{Lcl}}(R_{\text{lc}}R_{\text{l}} + X_{\text{lc}}X_{\text{le}})}{R_{\text{l}}{}^2 + X_{\text{le}}{}^2} \quad \text{(A14)}$$

$$K_{\phi 1 \text{k}} = (-1)^l \left(\frac{L_{\text{ke}}\cos(\Phi)}{L_{\text{ke}\phi}} - \frac{L_{\text{le}}}{L_{\text{le}\phi}} \frac{(R_{\text{lc}}R_{\text{l}} + X_{\text{lc}}X_{\text{le}})\cos(\Phi) + (X_{\text{lc}}R_{\text{l}} - R_{\text{lc}}X_{\text{le}})\sin(\Phi)}{R_{\text{l}}{}^2 + X_{\text{le}}{}^2} \right) \quad \text{(A15)}$$

$$K_{\phi 2 \text{k}} = (-1)^l \left(\frac{L_{\text{ke}}\sin(\Phi)}{L_{\text{ke}\phi}} - \frac{L_{\text{le}}}{L_{\text{le}\phi}} \frac{(R_{\text{lc}}X_{\text{le}} - X_{\text{lc}}R_{\text{l}})\cos(\Phi) + (R_{\text{lc}}R_{\text{l}} + X_{\text{lc}}X_{\text{le}})\sin(\Phi)}{R_{\text{l}}{}^2 + X_{\text{le}}{}^2} \right) \quad \text{(A16)}$$

$$\beta_{1\text{k}} = \frac{(R_{\text{l}}R_{\text{kc}} + X_{\text{le}}X_{\text{kc}})(R_{\text{lc}}X_{\text{ke}} - X_{\text{lc}}R_{\text{k}}) - (R_{\text{lc}}X_{\text{ke}} - X_{\text{lc}}R_{\text{k}})(R_{\text{lc}}R_{\text{k}} + X_{\text{lc}}X_{\text{ke}})}{(R_{\text{l}}{}^2 + X_{\text{le}}{}^2)(R_{\text{lc}}X_{\text{ke}} - X_{\text{lc}}R_{\text{k}}) - (R_{\text{lc}}{}^2 + X_{\text{lc}}{}^2)(R_{\text{l}}X_{\text{kc}} - X_{\text{le}}R_{\text{kc}})} \quad \text{(A17)}$$

V. Conclusions

A systematic reduced-order modeling approach for resonant inverters has been validated. It has been proved that SVAP and residualization technique from control systems theory for a series resonant capacitor provides identical results. A slight modification of SVAP, SVAPD approach has been proposed providing better dynamic results than residualization. This technique has been applied to a HBSRI and to a high-order plant a DHBSRI sharing resonant capacitor. For the first time, analytical transfer functions have been provided considering several control inputs and different outputs for a HBSRI and for a DHBSRI. After SVADP application, even the 6th order small-signal model of a DHBSRI obtained by EDF is reduced up to a simple 2nd order one. The validity range of the proposed models has been tested considering typical values of an induction heating application. The validity range extends up to a fifth of the resonance frequency showing its beneficial application for improving the controller robust performance in an application with such load uncertainty and variable operating condition. SVADP model order reduction technique has been applied considering several scenarios showing its easy extension to other resonant topologies, and more significantly to high-order plants.

VI. References

[1] S. R. Sanders, J. M. Noworolski, X. Z. Liu, and G. C. Verghese, "Generalized averaging method for power conversion circuits," Power Electronics, IEEE Transactions on, vol. 6, pp. 251-259, 1991.

[2] C. T. Rim and G. H. Cho, "Phasor transformation and its application to the DC/AC analyses of frequency phase-controlled series resonant converters (SRC)," Power Electronics, IEEE Transactions on, vol. 5, pp. 201-211, 1990.

[3] C. T. Rim, "Unified General Phasor Transformation for AC Converters," Power Electronics, IEEE Transactions on, vol. 26, pp. 2465-2475, 2011.

[4] S. Almer, S. Mariethoz, and M. Morari, "Dynamic Phasor Model Predictive Control of Switched Mode Power Converters," Control Systems Technology, IEEE Transactions on, vol. 23, pp. 349-356, 2015.

[5] Y. Yin, R. Zane, J. Glaser, and R. W. Erickson, "Small-signal analysis of frequency-controlled electronic ballasts," Circuits and Systems I: Fundamental Theory and Applications, IEEE Transactions on, vol. 50, pp. 1103-1110, 2003.

[6] C. Branas, F. J. Azcondo, and R. Zane, "Power-Mode Control of Multiphase Resonant Electronic Ballast," Industrial Electronics, IEEE Transactions on, vol. 59, pp. 1770-1778, 2012.

[7] Y. Tao, S. Bozhko, J. M. Le-Peuvedic, G. Asher, and C. I. Hill, "Dynamic Phasor Modeling of Multi-Generator Variable Frequency Electrical Power Systems," Power Systems, IEEE Transactions on, vol. 31, pp. 563-571, 2016.

[8] Y. Yan, R. Zane, R. Erickson, and J. Glaser, "Direct modeling of envelope dynamics in resonant inverters," in Power Electronics Specialist Conference, 2003. PESC '03. 2003 IEEE 34th Annual, 2003, pp. 1313-1318 vol.3.

[9] S. Jensen, L. Corradini, M. Rodriguez, and D. Maksimovic, "Modeling and digital control of LCLC resonant inverter with varying load," in Energy Conversion Congress and Exposition (ECCE), 2011 IEEE, 2011, pp. 3823-3829.

[10] E. X. Yang, F. C. Lee, and M. M. Jovanovic, "Small-signal modeling of series and parallel resonant converters," in Applied Power Electronics Conference and Exposition, 1992. APEC '92. Conference Proceedings 1992., Seventh Annual, 1992, pp. 785-792.

[11] S. Tian, F. C. Lee, and Q. Li, "A Simplified Equivalent Circuit Model of Series Resonant Converter," Power Electronics, IEEE Transactions on, vol. 31, pp. 3922-3931, 2016.

[12] G. C. Verghese, M. E. Elbuluk, and J. G. Kassakian, "A General Approach to Sampled-Data Modeling for Power Electronic Circuits," Power Electronics, IEEE Transactions on, vol. PE-1, pp. 76-89, 1986.

[13] W. Xuanlv, X. Guochun, and L. Bo, "Simplified Discrete-Time Modeling for Convenient Stability Prediction and Digital Control Design," Power Electronics, IEEE Transactions on, vol. 28, pp. 5333-5342, 2013.

[14] L. Grajales and F. C. Lee, "Control system design and small-signal analysis of a phase-shift-controlled series-resonant inverter for induction heating," in Power Electronics Specialists Conference, 1995. PESC '95 Record., 26th Annual IEEE, 1995, pp. 450-456 vol.1.

[15] A. Dominguez, A. Otin, L. A. Barragan, O. Lucia, and J. I. Artigas, "Modeling of resonant inverters with high harmonic content using the extended describing function method," in IECON 2012 - 38th Annual Conference on IEEE Industrial Electronics Society, 2012, pp. 5949-5954.

[16] A. Dominguez, L. A. Barragan, A. Otin, J. I. Artigas, I. Urriza, and D. Navarro, "Small-signal model of dual half-bridge series resonant inverter sharing resonant capacitor for domestic induction heating," in Industrial Electronics Society, IECON 2014 - 40th Annual Conference of the IEEE, 2014, pp. 3277-3282.

[17] J. Tian, J. Petzoldt, T. Reimann, M. Scherf, and G. Berger, "Modelling of asymmetrical pulse width modulation with frequency tracking control using phasor transformation for half-bridge series resonant induction cookers," in Power Electronics and Applications, 2005 European Conference on, 2005, pp. 9 pp.P.1-P.9.

[18] J. Tian, J. Petzoldt, T. Reimann, M. Scherf, and G. Berger, "Control system analysis and design of a resonant inverter with the variable frequency variable duty cycle scheme," in Power Electronics Specialists Conference, 2006. PESC '06. 37th IEEE, 2006, pp. 1-5.

[19] J. Tian, G. Berger, T. Reimann, M. Scherf, and S. J. Petzoldt, "Design and Implementation of a FPGA-Based Controller for Resonant Inverters," in Power Electronics Specialists Conference, 2007. PESC 2007. IEEE, 2007, pp. 779-784.

[20] F. H. Dupont, C. Rech, R. Gules, and J. R. Pinheiro, "Reduced-Order Model and Control Approach for the Boost Converter With a Voltage Multiplier Cell," Power Electronics, IEEE Transactions on, vol. 28, pp. 3395-3404, 2013.

[21] J. W. Kimball and P. T. Krein, "Singular Perturbation Theory for DC-DC Converters and Application to PFC Converters," Power Electronics, IEEE Transactions on, vol. 23, pp. 2970-2981, 2008.

[22] J. Sun and H. Grotstollen, "Averaged modeling and analysis of resonant converters," in Power Electronics Specialists Conference, 1993. PESC '93 Record., 24th Annual IEEE, 1993, pp. 707-713.

[23] S. Jian, D. M. Mitchell, M. F. Greuel, P. T. Krein, and R. M. Bass, "Averaged modeling of PWM converters operating in discontinuous conduction mode," Power Electronics, IEEE Transactions on, vol. 16, pp. 482-492, 2001.

[24] T. Pavlovic, T. Bjazic, and Z. Ban, "Simplified Averaged Models of DC-DC Power Converters Suitable for Controller Design and Microgrid Simulation," Power Electronics, IEEE Transactions on, vol. 28, pp. 3266-3275, 2013.

[25] S. Skogestad and I. Postlethwaite, Multivariable Feedback Control: Analysis and Design: Wiley-Interscience, 2005.

[26] N. Femia, G. Spagnuolo, and V. Tucci, "State-space models and order reduction for DC-DC switching converters in discontinuous modes," Power Electronics, IEEE Transactions on, vol. 10, pp. 640-650, 1995.

[27] A. Dominguez, L. A. Barragan, J. I. Artigas, A. Otin, I. Urriza, and D. Navarro, "Reduced-order model of a half-bridge series resonant inverter for power control in domestic induction heating applications," in Industrial Technology (ICIT), 2015 IEEE International Conference on, 2015, pp. 2542-2547.

[28] A. A. Aboushady, K. H. Ahmed, S. J. Finney, and B. W. Williams, "Linearized Large Signal Modeling, Analysis, and Control Design of Phase-Controlled Series-Parallel Resonant Converters Using State Feedback," Power Electronics, IEEE Transactions on, vol. 28, pp. 3896-3911, 2013.

[29] N. Ha Pham, H. Fujita, K. Ozaki, and N. Uchida, "Phase Angle Control of High-Frequency Resonant Currents in a Multiple Inverter System for Zone-Control Induction Heating," Power Electronics, IEEE Transactions on, vol. 26, pp. 3357-3366, 2011.

VII. Biographies

Alberto Dominguez (S'12) received the M. Sc. Degree in electronic engineering from the University of Zaragoza, Spain, in 2011. He is currently working toward the Ph.D. degree in the Department of Electronic engineering and Communications, University of Zaragoza. His main research interests include modeling, control and optimization of systems with constraints, especially devoted to resonant inverters in domestic induction heating. He is currently a member of the Aragon Institute for Engineering Research (I3A), Group of Power Electronics and Microelectronics (GEPM).

Luis A. Barragán received the M.Sc. and Ph.D. degrees in physics from the University of Zaragoza, Zaragoza, Spain, in 1988 and 1993, respectively. He is an Associate Professor with the Department of Electronic Engineering and Communications, University of Zaragoza. He has been involved in different research and development projects on induction-heating systems for home appliances. His research interests include modeling and digital control applied to domestic induction heating. Dr. Barragán is a member of the Aragon Institute for Engineering Research (I3A), Group of Power Electronics and Microelectronics (GEPM).

José I. Artigas received the M.Sc. and Ph.D. degrees in electrical engineering from the University of Zaragoza, Zaragoza, Spain, in 1989 and 1996, respectively. He has been with the Department of Electronic Engineering and Communications, University of Zaragoza, where he is currently an Associate Professor. He has been involved in different research and development projects. His main research interests include signal acquisition, digital control, and modulation strategies applied to power converters. Dr. Artigas is a member of the Aragón Institute for Engineering Research (I3A), Group of Power Electronics and Microelectronics (GEPM).

Aranzazu Otin (M'08) received the M.Sc. degree in Physics in 2001 and Ph.D. degree in Electronics Engineering in 2007 from the University of Zaragoza, Spain. She is an Associate Professor in the Department of Electronic Engineering and Communications, University of Zaragoza. Dr. Otin is a member of the Aragon Institute for Engineering Research (I3A), Group of Power Electronics and Microelectronics (GEPM). Her research interests include high performance microelectronics design, especially low power analog and mixed-signal ASIC design, and control strategies of inverters for induction-heating applications. She is currently involved in different research and development projects on induction-heating systems for home appliances.

Isidro Urriza received the M.Sc. and Ph.D. degrees in Electrical Engineering from the University of Zaragoza, Spain in 1991 and 1998, respectively. He has been with the Department of Electronic Engineering and Communications at the University of Zaragoza, Spain, where he is currently an Associate Professor. He has been involved in different research and development projects. His main research interests include digital implementation of modulation techniques for power converters. Dr. Urriza is a member of the Aragon Institute for Engineering Research (I3A), Group of Power Electronics and Microelectronics (GEPM).

Denis Navarro received the M.Sc. degree in microelectronics from the University of Montpellier II ,Montpellier, France, in 1987, and the Ph.D. degree from the University of Zaragoza, Zaragoza, Spain, in 1992. Since September 1988, he has been with the Department of Electronic Engineering and Communications at the University of Zaragoza, where he currently an Associate Professor. His current research interests include FPGA-based supercomputer, ASIC design, and modulation techniques for power converters. He is involved in the implementation of new applications of integrated circuits. In 1993, he designed the first SPARC microprocessor in Europe. Dr. Navarro is a Member of the Aragon Institute for Engineering Research (I3A), Group of Power Electronics and Microelectronics (GEPM).